



# Low-Dose Ionizing $\gamma$ -Radiation Elicits the Extrusion of Neutrophil Extracellular Traps

Alvaro Teijeira<sup>1,2,3</sup>, Saray Garasa<sup>1</sup>, Maria C. Ochoa<sup>1,2,3</sup>, Sandra Sanchez-Gregorio<sup>1</sup>, Gabriel Gomis<sup>1</sup>, Carlos Luri-Rey<sup>1</sup>, Rafael Martinez-Monge<sup>2,4</sup>, Beatrice Pinci<sup>1</sup>, Karme Valencia<sup>2,3,5</sup>, Belen Palencia<sup>1</sup>, Benigno Barbés<sup>6</sup>, Elixabet Bolaños<sup>1,2,3</sup>, Arantza Azpilikueta<sup>1,2,3</sup>, Marina García-Cardosa<sup>7</sup>, Javier Burguete<sup>2,7</sup>, Iñaki Eguren-Santamaría<sup>1,2,8</sup>, Eneko Garate-Soraluze<sup>1</sup>, Pedro Berraondo<sup>1,2,3</sup>, Jose L. Perez-Gracia<sup>2,8</sup>, Carlos E. de Andrea<sup>2,9,10</sup>, Maria E. Rodriguez-Ruiz<sup>1,2,3,11</sup>, and Ignacio Melero<sup>1,2,3,11,12</sup>

## ABSTRACT

**Purpose:** Patients with cancer frequently undergo radiotherapy in their clinical management with unintended irradiation of blood vessels and copiously irrigated organs in which polymorphonuclear leukocytes circulate. Following the observation that such low doses of ionizing radiation are able to induce neutrophils to extrude neutrophil extracellular traps (NET), we have investigated the mechanisms, consequences, and occurrence of such phenomena in patients undergoing radiotherapy.

**Experimental Design:** NETosis was analyzed in cultures of neutrophils isolated from healthy donors, patients with cancer, and cancer-bearing mice under confocal microscopy. Cocultures of radiation-induced NETs, immune effector lymphocytes, and tumor cells were used to study the effects of irradiation-induced NETs on immune cytotoxicity. Radiation-induced NETs were intravenously injected to mice for assessing their effects on metastasis. Circulating NETs in irradiated patients with cancer were

measured using ELISA methods for detecting MPO-DNA complexes and citrullinated histone 3.

**Results:** Irradiation of neutrophils with very low  $\gamma$ -radiation doses (0.5–1 Gy) elicits NET formation in a manner dependent on oxidative stress, NADPH oxidase activity, and autocrine IL8. Radiation-induced NETs interfere with NK cell and T-cell cytotoxicity. As a consequence, preinjection of irradiation-induced NETs increases the number of successful metastases in mouse tumor models. Increases in circulating NETs were readily detected in two prospective series of patients following the first fraction of their radiotherapy courses.

**Conclusions:** NETosis is induced by low-dose ionizing irradiation in a neutrophil-intrinsic fashion, and radiation-induced NETs are able to interfere with immune-mediated cytotoxicity. Radiation-induced NETs foster metastasis in mouse models and can be detected in the circulation of patients undergoing conventional radiotherapy treatments.

See related commentary by Mowery and Luke, p. 3965

## Introduction

Neutrophil extracellular traps (NET) result from the extrusion of nuclear chromatin from neutrophils. This form of cell death, termed

NETosis, is reportedly involved in microbial defense against bacteria and fungi (1). NET formation is elicited by microbial moieties such as lipopolysaccharide (2), but other factors are conducive to the extrusion of NETs, including chemokines (CXCR1/2 agonists; refs. 3–5), alarmins (HMGB1; ref. 6), and oxidative free radical species (7). The extracellular chromatin constituting the NETs adsorbs granular and cytoplasmic polypeptides that are endowed with antibiotic properties (8). For NETosis to occur, the contribution of protein arginine deiminase 4 (PAD4; ref. 2), the enzymatic function of which citrullinates histone 3 (9) to elicit chromatin decondensation, is crucial. Myeloperoxidase and granular proteases such as neutrophil elastase are reportedly also critical for NET formation (10). NETosis and NETs have been described to be involved in the pathogenesis of a broad spectrum of inflammatory, autoimmune, and vascular conditions (1, 11, 12).

In patients with cancer, NET formation has been described in tissue (13), and detectable concentrations of DNA tethered to myeloperoxidase or neutrophil elastase are often found in the circulation of patients suffering advanced hematologic (14) or solid malignancies (15). Circulating NETs are also characterized by citrullinated histone 3 (CitH3). Experiments performed in mouse models have revealed a role for NET formation in facilitating cancer metastases at various steps of the metastatic cascade (16), including extravasation (16), tissue invasion (16, 17), and preconditioning of the premetastatic niche (18). Moreover, direct effects of NETs on malignant cells have been described and are related to awakening dormancy (19) and other protumoral activities (20). Recent

<sup>1</sup>Program of Immunology and Immunotherapy, Cima Universidad de Navarra, Pamplona, Spain. <sup>2</sup>Navarra Institute for Health Research (IDISNA), Pamplona, Spain.

<sup>3</sup>Centro de Investigación Biomédica en Red de Cáncer (CIBERONC), Madrid, Spain.

<sup>4</sup>Department of Radiation Oncology, Clínica Universidad de Navarra, Pamplona, Spain. <sup>5</sup>Solid Tumors Program, Center for Applied Medical Research (CIMA), Pamplona, Spain.

<sup>6</sup>Department of Radiation Physics and Radiation Protection, Clínica Universidad de Navarra, Pamplona, Spain. <sup>7</sup>Department of Physics and Applied Mathematics, Universidad de Navarra, Pamplona, Spain. <sup>8</sup>Department of Medical Oncology, Universidad de Navarra, Pamplona, Spain.

<sup>9</sup>Department of Pathology, Clínica Universidad de Navarra, Pamplona, Spain. <sup>10</sup>Department of Anatomy, Physiology and Pathology, Universidad de Navarra, Pamplona, Spain. <sup>11</sup>Department of Immunology and Immunotherapy, Clínica Universidad de Navarra, Pamplona, Spain.

<sup>12</sup>Nuffield Department of Medicine, University of Oxford, Oxford, United Kingdom.

A. Teijeira and S. Garasa share first authorship of this article.

M.E. Rodriguez-Ruiz and I. Melero share senior authorship of this article.

**Corresponding Author:** Ignacio Melero, CIMA, Universidad de Navarra, Pio XII 55, Pamplona 31008, Spain. E-mail: imelero@unav.es

Clin Cancer Res 2024;30:4131–42

doi: 10.1158/1078-0432.CCR-23-3860

This open access article is distributed under the Creative Commons Attribution-NonCommercial-NoDerivatives 4.0 International (CC BY-NC-ND 4.0) license.

©2024 The Authors; Published by the American Association for Cancer Research

## Translational Relevance

We have discovered that low doses of ionizing radiation intrinsically induce the extrusion of the nuclear DNA from cultured neutrophils to form neutrophil extracellular traps (NET) as a result of mechanisms that depend on oxidative stress and NADPH oxidase activity. NETs are known to promote several aspects of cancer biology favoring tumor progression and metastasis, including cancer-associated immunosuppression. Radiotherapy, which is a treatment modality yearly experienced by millions of patients with cancer worldwide, induces NET formation (NETosis) at radiation doses that are received by a significant fraction of circulating polymorphonuclear leukocytes. Evidence in patients with cancer for increases in circulating NETs upon receiving the first fractions of radiotherapy courses is reported.

studies have found immunosuppressive functions for NETs, such as interference with NK cell and T-cell cytotoxicity in the effector phase (4). In line with this, NETs bear a constitutively active arginase 1 fragment that mediates immunosuppression (21). Following irradiation of experimental prostate cancer in mice, tissue specimens show increased contents of NETs, in which NET induction was dependent on HMGB1 release from dying tumor cells. In that experimental setting, NETs reduce T-cell infiltration and activity, thereby interfering with the efficacy of radioimmunotherapy strategies in this mouse model (22). Here, we show and mechanistically study a neutrophil-intrinsic mechanism of NETosis elicited by low-dose ionizing radiation.

## Materials and Methods

### Human studies

Human neutrophils, T cells, and NK cells were obtained from the peripheral blood of donors from a database mainly composed of graduate students (male and female, young adults) of Universidad de Navarra (Pamplona, Spain) following written, signed, and dated informed consent according to a protocol approved by the Institutional Ethics Committee. In some cases, neutrophils were isolated from the blood of patients with cancer from Clinica Universidad de Navarra (Pamplona, Spain) following written, signed, and dated informed consent. Patients of both sexes and different ages and with various types of cancer were included in the study, provided that they had been treated with radiotherapy and samples were available for the analyzed time points. All relevant information about patients with cancer included in the study is provided in Supplementary Table S1. All procedures and human data management have been performed according to protocols approved by the Institutional Ethics Committee (111/2010 and 2019-76) and upon informed consent according to Spanish and European regulations and in accordance with the Declaration of Helsinki. To ensure that subjects included in the study were representative, patients were not selected, and samples were taken from patients with cancer who had to undergo radiotherapy for their disease management within the radiotherapy service of Clinica Universidad de Navarra.

### Tumor cell lines and primary cultures

The HT29 cell line (RRID:CVCL\_0323) was obtained from the ATCC in 2011 and retrieved from the verified master cell bank

and cultured in RPMI (Gibco) complete media [10% FBS (Sigma) and 1% penicillin/streptomycin (Gibco)]. The 4T1 breast carcinoma cells (RRID:CVCL\_0125, female cells) of BALB/c origin were originally provided by Dr. Claude Leclerc, Institute Pasteur, and verified in the master cell bank at Institute Pasteur. The 4T1mCH cells were generated by Lipofectamine 2000 (Thermo Fisher Scientific) transfection with pCAGGS-mCherry (RRID:Addgene\_41583), as previously described (4). The cell lines were cultured in complete media containing RPMI 1640 medium (Gibco) supplemented with 10% FBS (Sigma-Aldrich), 100 IU/mL penicillin and 100 µg/mL streptomycin (Gibco), and  $5 \times 10^{-5}$  mol/L 2-mercaptoethanol (Gibco). All cell lines were grown in a humidified incubator with 5% CO<sub>2</sub> at 37°C for at least 7 days before inoculation into mice. All cell lines were routinely tested (every 2 weeks) for *Mycoplasma* contamination using the MycoAlert *Mycoplasma* detection kit (Lonza). Cells were kept in a master bank in large stocks to ensure minimal passaging. Cells were used in experiments after two to four passages after thawing from the master bank.

For neutrophil enrichment, peripheral blood samples drawn in heparin-containing tubes were subjected to Ficoll separation. Erythrocytes and neutrophil-containing pellets were then mixed with one volume of cold PBS and an extra volume of 6% dextran/0.9% NaCl solution. After being inverted 18 to 20 times to ensure adequate mixing, the mixture was placed upright at room temperature (RT) for 1 hour until phase separation was complete. The yellowish supernatant was recovered into a 50-mL tube and spun at 1,200 rpm for 12 minutes at 4°C. The supernatant was then discarded, and the pellet was resuspended in 5 mL ACK buffer for 5 minutes at RT to lyse erythrocytes. After incubation, the cells were washed with 45 mL of cold PBS. The supernatant was discarded, and the pellet was suspended in Hank's Balanced Salt Solution (HBSS) for further experiments.

Mouse neutrophils were immunomagnetically isolated from the spleens and bone marrow (BM) of mice carrying 21-day bilateral 4T1 tumors using the Ly6G microbead kit (Miltenyi) according to the manufacturer's instructions.

Human T and NK lymphocytes were obtained from peripheral blood mononuclear cells of healthy donors isolated from total blood by Ficoll gradients. To activate T cells, peripheral blood mononuclear cells were incubated with plates bound with anti-CD3 (OKT3, 1 µg/mL, BioLegend, RRID:AB\_571926) and 5 µg/mL of soluble anti-CD28 (clone CD28.2, BioLegend, RRID:AB\_314303). After 48 hours, cells were recovered, centrifuged, and resuspended at 10<sup>6</sup> cells/mL in RPMI complete media supplemented with hIL2 (25 U/mL, ImmunoTools). Such cultures were used in experiments between days 7 and 10 of culture. Human NK cells were isolated by negative magnetic selection using an EasySep human NK cell isolation kit (STEMCELL). NK cells were cultured on plates coated with human IgG (Beriglobin) at 50 µg/mL in NK MACS medium (Miltenyi) supplemented with 5,000 U/mL of IL2 and 5% human serum. NK cells were used for cytotoxicity assays after 48 hours of culture.

### NET formation assays

Neutrophils were resuspended in HBSS (Gibco). Cells ( $2 \times 10^5$ ) were then placed in 150 µL of HBSS, irradiated in a Nordion Gammacell 3000 irradiator to receive the indicated doses, and placed in eight-well uncoated ibidi microscopy chambers (ibidi). Stimuli and inhibitors were added on top at the following

concentrations unless indicated in the figure or figure legends: N-acetylcysteine (NAC; Sigma), 5 mmol/L; ethylene glycol tetraacetic acid (EGTA) (Sigma), 0.1  $\mu\text{mol/L}$ ; anti-IL8 (BMS-986253), 10  $\mu\text{g/mL}$ ; GSK484 (MedChem Plus), 5  $\mu\text{mol/L}$ ; Ptx (Tocris), 150 ng/mL; DNase I (Pulmozyme, Roche), 0.25 U; reparixin, 0.5  $\mu\text{mol/L}$  (Dompé Pharma); diphenyleneiodonium (DPI) 0.1  $\mu\text{mol/L}$  (Sigma); human albumin, 1.33 mg/mL (Sigma); and recombinant human thioredoxin (Bio-Techne). Cells were incubated for 4 hours at 37°C and 5% CO<sub>2</sub>, and SYTOX Green (25 nmol/L, Thermo Fisher Scientific) was added to the mixture and incubated for 5 minutes. Cells were paraformaldehyde (PFA)-fixed by adding 50  $\mu\text{L}$  of 16% PFA (Thermo Fisher Scientific) and kept at 4°C until confocal microscopy was performed.

Confocal microscopy was performed to quantify NET formation. Z-stacks of 10 to 30  $\mu\text{m}$  depths captured at 40 $\times$  magnification were taken in an LSM800 microscope equipped with a 488 diode and a Plan-Apochromat 40 $\times$  1 N/A Oil DIC III objective. Fiji software and the particle analyzer plugin were used for the quantification of the area occupied by NETs. Only structures depicting NET morphology and positivity for SYTOX Green were selected for area quantification, whereas intact granulocyte nuclei were excluded from the analysis.

#### Degranulation assessment by flow cytometry

Neutrophils were resuspended in HBSS (Gibco). Cells ( $2 \times 10^5$ ) were then placed in 150  $\mu\text{L}$  HBSS, irradiated in a Nordion Gammacell 3000 irradiator with the indicated doses, and then cultured for additional 30 minutes. Irradiated (10 Gy) neutrophils treated with Nexinhib20 (66  $\mu\text{mol/L}$ ) were taken as a negative control, and neutrophils treated with 1  $\mu\text{mol/L}$  fMLP (Sigma) were taken as a positive control. After such culture, cells were centrifuged and stained with the following Abs: anti-hCD15 BV510 (AB\_2738025), anti h/m CD11b Percp-Cy5.5 (AB\_2738025), anti-CD66b AF647 (AB\_2563170; all from BioLegend), and anti-CD63 BV421 (AB\_2687003). Cells were analyzed using a CytoFLEX S flow cytometer (Beckman Coulter).

#### Reactive oxygen species generation assessment by Amplex red

Neutrophils ( $2 \times 10^5$ ) were resuspended in 50  $\mu\text{L}$  HBSS (Gibco), and 50  $\mu\text{L}$  of Amplex red/horseradish peroxidase (Thermo Fisher Scientific) working solution was added according to the manufacturer's instructions. The fluorescence was measured at multiple points following the kinetics of the reaction in a FLUOstar plate reader (BMG).

#### Tumor spheroid cultures

Tumor-derived spheroids from HT29 colon cell lines were derived, as explained elsewhere (4). Briefly,  $1.5 \times 10^4$  cells were cultured in 25  $\mu\text{L}$  of Matrigel (Corning) in the presence of advanced DMEM/F12 (Gibco). Cells were cultured for 5 to 6 days before video microscopy or cytotoxicity experiments.

#### Time-lapse confocal microscopy

For all video microscopy experiments, time-lapse videos were taken in an LSM 880 microscope (Zeiss) equipped with an incubator with controlled temperature (37°C) and CO<sub>2</sub> (5%).

For tumor spheroids covered by NETs in cocultures with NK or T cells, 5-day tumor spheroids were recovered from Matrigel and stained with CellTracker Orange CMRA (Thermo Fisher Scientific; 20 minutes 37°C). Cytotoxic cells were stained with CellTracker Deep Red (Thermo Fisher Scientific), as previously explained. Five-

day tumor spheroids were cocultured with neutrophils previously irradiated with 2 Gy  $\gamma$ -radiation for 4 hours in HBSS in the presence or absence of DNase I (0.25 U, Pulmozyme, Roche). Subsequently, spheroids were recovered, centrifuged, and cocultured with  $2 \times 10^5$  prestained cytotoxic T-cell or NK cell lymphocytes in 10% Matrigel/10% collagen type I (PureCol, Advanced BioMatrix)/80% RPMI supplemented with 50 nmol/L SYTOX Green on eight-well microscopy chambers (Labtek). Plates were cultured for 4 hours at 37°C to allow gelification before image acquisition. Time-lapse z-stack videos were taken every 60 seconds for 8 hours for each condition with a 25 $\times$  water immersion objective LD LCI Plan-Apochromat 25 $\times$  0.8 N/A. Videos were analyzed using Imaris software (Oxford Instruments). Semiautomatic tracking of cytotoxic cells was performed using the spot function, and tumor spheroids were segmented using the surface functions. Minimum distances of each cytotoxic cell track to segmented tumor spheroids were quantified to account for effector lymphocyte/tumor-cell contacts.

To assess NETosis by live microscopy, human neutrophils were prestained with CMRA (Thermo Fisher Scientific) for 20 minutes at 37°C in RPMI (Gibco). A sum of 150,000 neutrophils were resuspended in HBSS containing SYTOX Green (25 nmol/L), subjected to the indicated doses of  $\gamma$ -irradiation and placed in eight-well ibidi plates. Z-stack acquisition was performed every 2 to 7 minutes for 5 hours. To acquire images, a 25 $\times$  LD LCI Plan-Apochromat 0.8 Oil/Glyc/W Corr DIC objective was used. The number of NETosis events in time-lapse videos was quantified by segmenting the SYTOX Green-positive signal using Imaris (RRID:SCR\_007370), excluding those cells that did not undergo NETosis upon SYTOX Green uptake.

#### Mouse studies

Mice were housed at the animal facility of the CIMA, Universidad de Navarra (Pamplona, Spain). Six-week-old female and male C57BL/6 (RRID:MGI:2161072) and BALB/c (RRID:IMSR\_JAX:000664) mice were purchased from Envigo. All animal procedures were approved by the Institutional Animal Experimentation Ethics Committee and the regional government of Navarra (protocols 037-19 and 132-22). The ages of mice included in experiments ranged from 8 to 12 weeks.

For 4T1 metastasis studies, NETs were isolated from the supernatant of  $20 \times 10^6$  human neutrophils irradiated with 2 Gy of  $\gamma$ -radiation, as previously described (23, 24). Briefly, HBSS was carefully removed, and the plates were washed with 1 mL of ice-cold PBS. These NET-rich supernatants were centrifuged for 10 minutes at 450 g at 4°C to eliminate neutrophil remains and were kept frozen until the day of the experiment. Before injection, the NET-rich supernatant was thawed and subjected to mild sonication (three 30-second cycles at 4°C, high frequency) on a Bioruptor<sup>®</sup> sonicator (Diagenode), and the DNA concentration was quantified using a NanoDrop spectrophotometer (Thermo Fisher Scientific). Balb/c mice were preinjected intravenously with 660 ng of NET-DNA 48 hours and 24 hours before intravenous tumor cell injection. In some cases, 25 U of DNase I was added to such NETs and incubated for 10 minutes at 37°C before intravenous injection. The following morning,  $2.5 \times 10^4$  4T1 mCherry tumor cells were intravenously injected via the tail vein. For NK depletion, 50  $\mu\text{g}$  of anti-Asialo GM1 (Wako Fujifilm, AB\_516844) was intravenously injected on days 4 and 2 before tumor cell i.v. injection, and 200  $\mu\text{g}$  of anti-CD8 $\beta$  (clone Lyt3.2, Bio X Cell, AB\_2687706) was intraperitoneally injected 48 hours before intravenous 4T1mCH tumor cell injection. Ten days after intravenous tumor cell injection, lungs

were collected, and epifluorescence images were taken of the whole lungs using a ChemiDoc imaging system (Bio-Rad) with the appropriate filter sets. The tumor cell area was measured using Fiji software.

Experiments on the spontaneous metastasis model were performed as follows:  $5 \times 10^4$  of mCherry-4T1 cells were orthotopically injected into the fourth left mammary fat pad of 8-week-old female BALB/c mice. On day 13 after tumor cell injection, contralateral fat pads were subjected to 6 Gy of irradiation for 3 consecutive days using a small radiation research platform (Xstrahl, Inc.). A group of irradiated mice was treated with three doses 50 mg of the PAD4 inhibitor GSK484 (MedChem Plus). Other mice were left untreated or were injected with 660 ng of radiation-induced NET-DNA at days 13, 14, and 15 posttumor injection. Tumors were excised from the mammary fat pad on day 16. On day 38, mice were sacrificed, lungs were excised, and epifluorescence images of the lungs were taken using a Leica inverted fluorescent microscope. At least three representative fluorescence images were acquired at  $20\times$  magnification from each individual mCherry+ tumor-metastasized organ. The percentage of the surface area from the organs occupied by the metastasized tumor was assessed using Fiji image software (RRID:SCR\_002285). The mean metastasis area was estimated for each individual organ.

#### Immunofluorescence studies of mouse tissue

For whole-mount immunofluorescence of mouse BM, we followed a previously published protocol (25). 4T1 tumor-bearing mice or naïve mice were subjected to total body irradiation (TBI) with the indicated doses. Four hours later, mice were perfused with 4% PFA, and their bones were collected and postfixed for an additional 24 hours in 4% PFA at  $4^\circ\text{C}$ . The bones were then embedded in optimal cutting temperature compound (OCT), and a Microm cryostat (HM520) was used to cut the bone until the BM was exposed (25). Then, the bones with their BM exposed were incubated in cold PBS for 2 hours with gentle agitation to remove OCT. Bones were then recovered and stained overnight at  $4^\circ\text{C}$  in a buffer made of 1% BSA and 0.05% saponin in PBS with the following Abs: anti-mLy6GPE (BioLegend, AB\_1186104), anti-mouse CD31 AF488 (BioLegend, AB\_2161031), and rabbit anti-human/mouse CitH3 R2+R8+R17 (Abcam, AB\_304752). The bones were then thoroughly washed and stained in the very same buffer with a donkey anti-rabbit AF647 polyclonal Ab (Thermo Fisher Scientific) for an additional 24 hours. The bones were washed, briefly incubated with Hoescht (1:1,000, Thermo Fisher Scientific), and placed in an ibidi 35-mm  $\mu$ -Dish to perform confocal microscopy in an LSM800 confocal microscope equipped with a  $40\times$  oil immersion objective. The total CitH3 area in Ly6G-positive cells was quantified in several microscopic fields using Imaris software.

For experiments including staining of BM aspirates, naïve and 4T1-bearing mice were subjected to TBI, as explained previously, and 4 hours later, BM was flushed, centrifuged, and treated with ACK lysis buffer for 1 minute. Cells were plated in eight-well ibidi chambers and then stained with SYTOX Green and in some instances, with anti-CitH3 Abs followed by an anti-rabbit 647 fluorescent Ab. Subsequently, NETs were analyzed by confocal microscopy, as previously explained. To study the effects on spleens after TBI, splenocytes were subjected to fast Ly6G<sup>+</sup> magnetic isolation immediately after mice TBI and cultured in HBSS for an additional 4 hours, as described previously.

#### Cytotoxicity assays

For cytotoxicity assays, HT29 5-day tumor spheroids were generated, recovered from Matrigel, and stained, as previously explained. Neutrophils ( $5 \times 10^5$ ) were stimulated with 2 Gy radiation  $\pm$  DNase I (0.25 U/mL) for 2 hours or left untreated in the appropriate controls. Then,  $5 \times 10^4$  tumor spheroids were added per well in 50  $\mu\text{L}$  of media. Two hours later, cocultures were collected, centrifuged, and mixed with  $1.5 \times 10^5$  T cells or prestained NK cells in 10% Matrigel, 10% collagen type I, and 80% RPMI. EpCAM BiTE (1  $\mu\text{g}/\text{mL}$ ; Creative Biolabs) was added when T cells were used in the cocultures. The cocultures were placed in 100  $\mu\text{L}$  in U-shaped 96-well plates. For flow cytometry analysis, cocultures were recovered 24 hours (in the case of cocultures with T cells) or 48 hours (in the case of cocultures with NK cells) later. For cell recovery, gels were resuspended with an additional ice-cold 100  $\mu\text{L}$  of PBS, incubated for 10 minutes at  $4^\circ\text{C}$ , and transferred to V-shaped 96-well plates. After centrifugation, the wells were treated with 50  $\mu\text{L}$  of TrypLE cell dissociation reagent (Gibco) for 15 minutes at RT. The cells were washed twice and stained with anti-hCD45 Pacific Blue (BioLegend, AB\_2174123), anti-hEpcam-Percp-Cy5.5 (AB\_2098808), anti-hCD8 APC (AB\_2616624), and Zombie NIR death cell staining (BioLegend) for 10 minutes in PBS containing 5% FBS unless cells had been prestained. The cells were analyzed in a CytoFLEX S cytometer (Beckman Coulter). Remaining neutrophils were excluded from the analysis on the basis of side scatter (SSC). As recovery of the gels showed variability, fluorescent tumor cell numbers were always normalized to recovered T cells or NK cells.

#### ELISAs of circulating NETs in patients with cancer and in mice

Blood samples were obtained by venipuncture from patients undergoing radiotherapy (Supplementary Table S1) following the specimen repository protocol from our institution (protocol number 111/2010). Cell-free serum samples were aliquoted and immediately stored at  $-80^\circ\text{C}$ .

Indirect quantification of NETs in serum was carried out by determining the MPO–DNA complexes and CitH3. Levels of CitH3 in human and mouse serum were measured using the Cayman Chemical ELISA kit (product # 501620, Cayman Chemical).

MPO–DNA complexes were determined by ELISA modifying the protocol previously described (26). As the capturing Ab, 5  $\mu\text{g}/\text{mL}$  of anti-MPO mAb (Clone 266-6K1, Hycult Biotechnology, AB\_533154) was used to coat 96-well microtiter plates (Ref. 10547781, Nunc) in 0.1 mol/L sodium carbonate buffer (pH 9.5) overnight at  $4^\circ\text{C}$ . After blocking in 1% BSA for 1 hour, patient serum diluted 1:2 in 1% BSA was added in combination with the peroxidase-labeled anti-DNA mAb (clone MCA-33, component No. 2 of the commercial cell death detection ELISA kit; Roche, Cat. No.: 11774425001) diluted 1:40. After 2 hours of incubation at RT on a shaking device, the samples were washed seven times with 0.1% Tween 20 in PBS. TMB substrate reagent (Ref. 555214, BD OptEIA) was added following the manufacturer's instructions, and when the first four wells of the standard showed changes in color (15–20 minutes), the reaction was stopped with sulfuric acid solution 2 N. The absorbance at 450 nm/L wavelength was measured using a Multiskan Ascent reader (Thermo). As a standard, NETs isolated from supernatants from irradiated neutrophils were used. A value of 100 U/mL was given to the crude standard, and seriated 1:2 dilutions were performed to plot a curve that was adjusted to a one-phase decay model to extrapolate the values of the samples.

The model adjustment was done using GraphPad Prism 8 software (RRID:SCR\_002798).

Patients that showed high levels of circulating NETs before radiotherapy (those in the highest quartile) were excluded from the analysis to avoid confusion with NETs induced by other factors besides irradiation.

IL8 levels were quantified using a commercially purchased ELISA kit, according to the manufacturer's instructions (product # 555244, BD Biosciences), on the supernatants of neutrophils recovered 10 minutes after  $\gamma$ -irradiation.

### Estimation of the volume of irradiated blood in patients with cancer

The radiation dose received in major vessels by the circulating blood was characterized by the dose received by individual droplets moving through the vascular tree. The arterial and venous vessels of each patient were contoured using the planning CT scan and, when available, other image series. The aorta, cava, and common external and internal iliac arteries and veins were selected from the anatomy of each case. The total blood volume for each patient was determined by their height and weight (27). This blood volume was divided into droplets of 1 mm<sup>3</sup> that circulate along each one of the four possible trajectories on this vasculature (through external or internal branches on the right or left side).

The circulating flow rate was estimated using the data published in Fronck and colleagues (28). In this article, the authors studied the common femoral hemodynamics for a large group of people and observed the ways in which the flow rate varies in different age and sex groups. The data on a male population at rest (mean: 16.6 cm<sup>3</sup>/second; SD: 7.2 cm<sup>3</sup>/second) were introduced into our model to quantify the blood circulating in the external iliac veins. That flow corresponds to only a part of the total blood circulating in the cava (mean: 85%; SD: 5%), with all the rest circulating through the internal iliac veins. The blood flow rates for the other vessels were obtained from these values. Using these flow rates and the vasculature volume, we were able to determine the spatial distribution of the time-averaged blood flow velocities throughout its trajectory.

For each trajectory, a spatial-dependent, time-averaged dose rate was obtained from the planning dose. The dose rate corresponds to the planning dose on each spatial position divided by the total irradiation time, which was obtained from the operator console.

The dose that a moving specific droplet receives was computed along the trajectory, using the spatial distribution of dose rates, multiplied by the time the droplet remained in a specific position. These droplets propagate along each one of the four different trajectories with a probability that corresponds to the relative value of the corresponding flow rate. This process was repeated until we reached the total irradiation time.

For each patient, we performed 100 different runs in which the flow rate and the ratio of external to internal flow rates were randomly varied according to the values presented previously. We recovered a distribution of doses received by each one of these droplets for the 100 different scenarios. With these data, we could recover different statistics for a single radiotherapy fraction, including the percentage of irradiated blood receiving at least the indicated irradiation doses.

### Quantification and statistical analysis

Data were processed using GraphPad Prism 6.0 (RRID:SCR\_002798). Flow cytometry analyses were performed using FlowJo\_V10 or CytExpert software (RRID:SCR\_017217). Means and SDs of the

mean are presented as averages and error bars as indicated in the figure legends. All experimental repetitions and numbers of specimens, mice, and subjects are indicated in the figure legends. Mann-Whitney *U*-tests or Kruskal-Wallis tests were generally used to analyze statistical differences between independent groups unless indicated. *P* values are shown for any relevant statistical differences in the figures.

### Data availability

All reanalyzable data are publicly available at Zenodo (RRID:SCR\_004129), <https://zenodo.org/records/10806435>. Any additional information required to reanalyze the data reported in this article is available from the lead contact upon request.

## Results

### Low-dose $\gamma$ -radiation induces NETosis

Radiotherapy is commonly used for treating patients with cancer delivering ablative doses on the tumoral lesions to destroy malignant cells. However, low doses of radiation are also received by vascularized organs surrounding the irradiated tumor lesions. With this notion in mind, we studied whether irradiation could induce NETosis on isolated human neutrophils cultured for short periods of 4 hours. As shown in **Fig. 1A**, isolated neutrophils from healthy volunteers or patients with advanced cancer undergo NETosis at doses of  $\gamma$ -radiation as low as 0.25 to 0.5 Gy. Such an effect was also substantiated when irradiating mouse neutrophils isolated from the spleen or BM of tumor-bearing animals (**Fig. 1B**). The mice bearing 4T1 engrafted tumors were used because they exhibit increased numbers of granulocytic myeloid-derived suppressor cells (29). Evidence for low-dose radiation-induced NETosis was also recorded using time-lapse confocal microscopy, as can be seen in videos in which prestained neutrophils were irradiated at low doses and cultured in the presence of a dye that detects extracellular DNA (**Fig. 1C**; Supplementary Video S1). These confocal microscopy results unequivocally show a progressive number of NETosis events almost completely dependent on irradiation, even at low doses (**Fig. 1C**). Moreover, CitH3<sup>+</sup> extracellular NETs were clearly detectable in BM aspirates from 4T1 tumor-bearing and tumor-naïve mice drawn as early as 4 hours after TBI with 1 Gy (TBI, 1 Gy; **Fig. 1D and E**). Such effects were recapitulated in cell suspensions of Ly6G-positive cells from the spleen of 4T1-bearing mice subjected to TBI (**Fig. 1F**). Whole-mount immunofluorescence of the BM of irradiated mice also shows that Ly6G neutrophils undergo radiation-dependent NETosis as detected by CitH3 staining (**Fig. 1G**). Furthermore, increased circulating concentrations of CitH3 were detected in 4T1-bearing mice treated with TBI (2 Gy doses) as early as 4 hours postirradiation (**Fig. 1H**).

### Low-dose $\gamma$ -radiation requires oxidative mechanisms and NADPH oxidase activity to induce NETosis

The next logical step was to investigate the molecular mechanisms underlying the induction of NETosis as surprisingly induced by such low doses of  $\gamma$ -irradiation. First, NETosis was induced in human neutrophils in the presence of various pharmacologic inhibitors reported to interfere with NETosis, at least in some instances. NETosis was inhibited by PAD4 inhibition (30), inhibitors of the CXCR1/2 receptors (31), an anti-IL8-neutralizing mAb (32), and the antioxidant agent NAC (ref. 33). Of note, pertussis toxin did not inhibit NET extrusion, whereas digestion of extracellular DNA with DNase I eliminated all the NET-dependent signals (**Fig. 2A**).

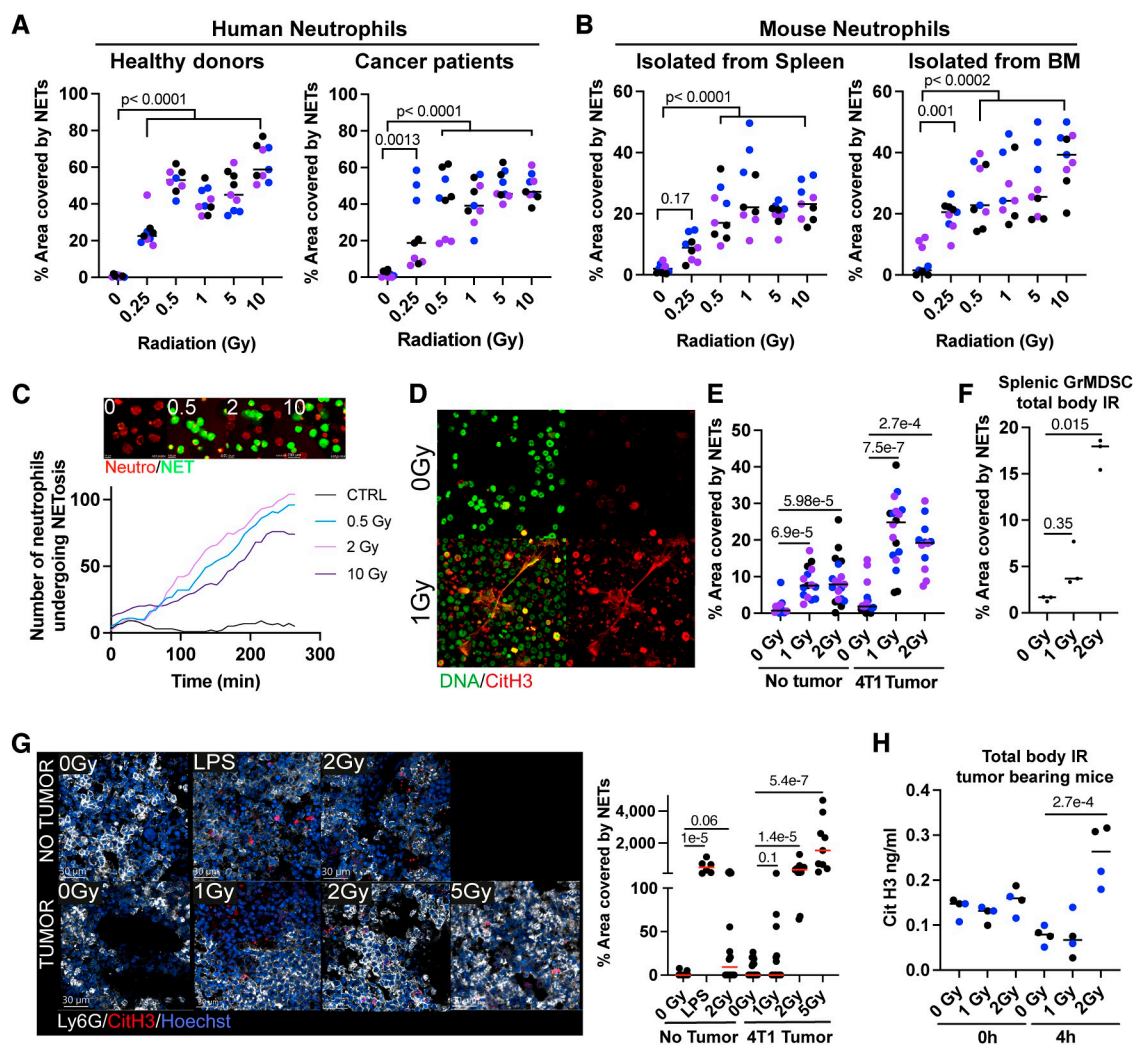


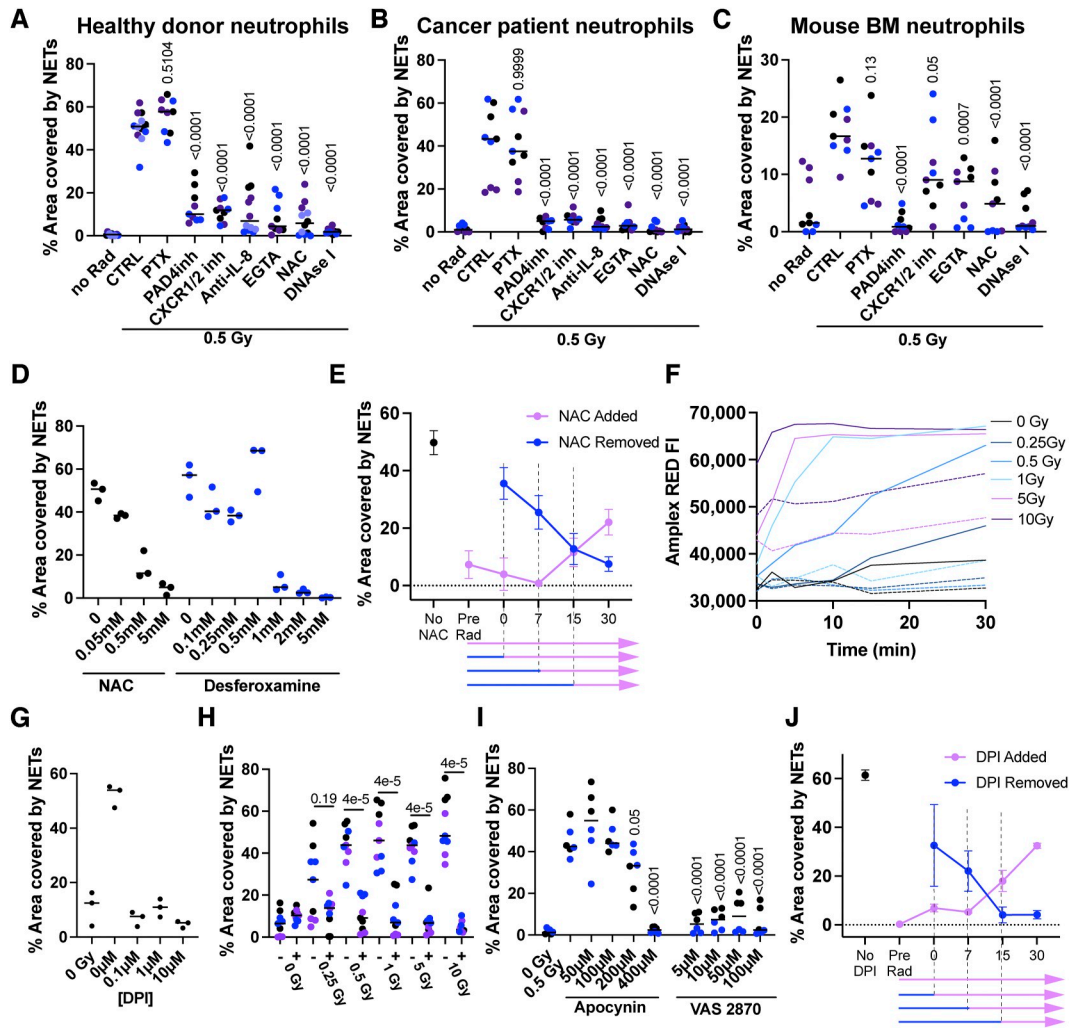
**Figure 1.**

NETosis induction by low-dose  $\gamma$ -irradiation on human and mouse neutrophils. Neutrophils were isolated from the blood of healthy human donors or heavily burdened patients with cancer (**A**) or the BM and spleen of mice bearing established 4T1 subcutaneous tumors (**B**), treated with the indicated  $\gamma$ -radiation doses, and NETosis was evaluated by SYTOX Green staining of extruded DNA by confocal microscopy. **C**, Curves over time of the fraction of neutrophils experiencing NETosis at the indicated time points following irradiation. Microphotographs of human neutrophils undergoing NETosis upon exposure to the indicated radiation doses from Supplementary Video S1. Representative frames of the 4-hour time point are shown above the graph. **D** and **H**, Tumor-naïve or mice bearing 4T1 subcutaneous tumors received TBI with the indicated  $\gamma$ -radiation doses, and 4 hours later, neutrophils from BM and blood were quantitatively analyzed for the presence of NETs. **D**, Representative confocal images showing SYTOX Green staining (green) and CitH3 (red) of cells in BM aspirates isolated from 4T1-bearing mice treated with the indicated  $\gamma$ -radiation doses. **E**, Quantification of images as in (**D**). **F**, NETosis assessment by SYTOX Green staining of neutrophils isolated from the spleen of 4T1 tumor-bearing mice treated with the indicated TBI dose. **G**, Whole-mount immunofluorescence of the BM of mice treated with TBI at the indicated doses and quantification of the NET area (CitH3<sup>+</sup> DNA). Neutrophils (Ly6G, white), CitH3 (red), and DNA (Hoechst, blue) are shown. **H**, ELISA quantification of circulating CitH3 concentrations in the serum of mice bearing 4T1 subcutaneous tumors treated with low-dose TBI. Kruskal-Wallis tests followed by *post hoc* tests were performed for multiple comparisons and Mann-Whitney *U*-tests for side-by-side comparisons. Differentially colored dots represent individual donors/mice.

Such results were recapitulated when using neutrophils obtained from patients with advanced cancer (**Fig. 2B**) or neutrophils from BM cell suspensions from tumor-bearing mice (**Fig. 2C**). The effect of IL8 blockade on human NETosis was to some extent surprising. However, we detected soluble IL8 in the supernatants of irradiated neutrophils (Supplementary Fig. S1A). The presence of such extracellular IL8 likely results from the mild neutrophil degranulation induced by irradiation (34) consistent with increases in surface

immunostaining for CD66b, CD63, and CD11b (Supplementary Fig. S1B), as reportedly occurs following degranulation (35). The auto-crine effect of IL8 took place mostly at early time points because CXCR1/2 inhibition with reparixin resulted in a reduction in NETosis when applied as early as 30 minutes postirradiation but not if provided at later time points (Supplementary Fig. S1C). We corroborated the importance of oxidative stress by testing another powerful antioxidant (deferoxamine) in NETosis assays and



**Figure 2.**

Mechanistic requirements for the induction of NETosis by low-dose radiation. **A** and **C**, NETosis assessment by SYTOX Green staining and confocal microscopy of cultured neutrophils isolated from the blood of healthy human donors (**A**), heavy-burden patients with cancer (**B**), or the BM of 4T1 tumor-bearing mice (**C**) *ex vivo* treated with 0.5 Gy of  $\gamma$ -radiation and the indicated pharmacologic inhibitors. **D**, NETosis assessment of healthy donor neutrophils treated with 0.5 Gy of  $\gamma$ -radiation and the indicated doses of antioxidant molecules. **E**, Human neutrophils were *ex vivo* treated with 0.5 Gy of  $\gamma$ -radiation, and 0.5 mmol/L of NAC was added or washed from the neutrophil cultures at the indicated time points. Then, cells were incubated for up to 4 hours, and NETs were quantified by SYTOX Green staining. **F**, ROS production assessments using Amplex red staining of neutrophils treated with the indicated  $\gamma$ -radiation doses over time. Dotted lines represent neutrophils treated with 0.5 mmol/L of NAC in addition to  $\gamma$ -radiation. NETosis assessment on human neutrophils treated with increasing concentrations of NADPH oxidase inhibitor DPI (**G**) or 0.1  $\mu$ mol/L DPI when receiving increasing doses of  $\gamma$ -radiation (**H**). **I**, NETosis assessments of healthy donor neutrophils treated with 0.5 Gy of  $\gamma$ -radiation and the indicated concentrations of NADPH oxidase inhibitors. **J**, Human neutrophils were treated with 0.5 Gy of  $\gamma$ -radiation, and 0.1  $\mu$ mol/L DPI was added or washed from the neutrophil cultures at the indicated time points as shown in (**E**). Kruskal-Wallis tests followed by *post hoc* tests were performed for multiple comparisons and Mann-Whitney *U*-tests for side-by-side comparisons. Differentially colored dots represent individual donors or individual mice.

observed again a concentration-dependent inhibition of radiation-induced NETosis (**Fig. 2D**). The effect of NAC was further explored in assays in which this compound was added or washed at different time points (**Fig. 2E**). These experiments showed that NAC was required at very early time points postirradiation, if it were to successfully inhibit NETosis. Consistent with the antioxidant effects of NAC, oxygen-free radicals were detected in the neutrophils using a fluorometric method as early as 1 to 2 minutes following  $\gamma$ -irradiation acting as an early triggering event (**Fig. 2F**). Of note, NAC is a chelator of hydroxyl free radicals and therefore would be

able to block reactive oxygen species (ROS) activity from both ROS induced directly by irradiation and any ROS secondarily produced by enzymes expressed by the neutrophils. Desferoxamine, however, is a Fe chelator, and would most likely only inhibit ROS production as induced by secondary enzymes but not the ones generated by ionizing radiation itself. In line with these observations, we hypothesized that radiation-induced ROS signaling could be further amplified by the main source of  $O_2^{+2}$  in the neutrophils, the NADPH oxidase system, which is causative of the respiratory burst (36). Indeed, NADPH activity is already known to be triggered by

oxidative stress (37). In accordance with these notions, the selective NADPH inhibitor DPI chloride blocks the NETosis induced by irradiation (Fig. 2G) as well as that induced by H<sub>2</sub>O<sub>2</sub> (Supplementary Fig. S1D). These results were confirmed in the presence of DPI across various radiation doses (Fig. 2H) and recapitulated with two other NADPH oxidase pharmacologic inhibitors, namely, apocynin and VAS2870 (Fig. 2I). The involvement of NADPH oxidase occurred at an early time point as concluded from the addition or retrieval of NADPH pharmacologic inhibition from the cultures. These effects mainly take place during 15 minutes postirradiation (Fig. 2J).

### Radiation-induced NETs interfere with immune cell cytotoxicity and promote metastasis

Low-dose irradiation-induced NET formation may exert immunomodulatory effects, among other protumor consequences. Following our published work (13), we studied if radiation-induced NETs can interfere with the lymphocyte-mediated cytotoxicity of human tumor spheroids. For this purpose, we used spheroids derived from the HT29 colon cancer cell line that were stained with a red tracker. Such spheroids, if incubated with irradiated neutrophils, were surrounded by the NET structures that could be stained with SYTOX Green (Fig. 3A). Performing confocal videomicroscopy of such tumor spheroids cocultured with T cells, we observed that T lymphocytes were not able to approach tumor cells when NETs were present and that this effect was lost when the NETs were digested by DNase I during the cocultures (Fig. 3A and B; Supplementary Video S2). In five similar cocultures in which T cells were redirected to kill tumor cells by a T-cell engager using an EpCAM-CD3 bispecific Ab, undigested NETs were partially protected from cytotoxicity as assessed by the recovery of living tumor cells from the cocultures (Fig. 3C). Similar experiments were performed using activated human NK cells as cytotoxic effectors, in this case without the need to redirect the killing. In such NK cytotoxicity experiments, protection against killing by the radiation-induced NETs was again substantiated (Fig. 3D-F; Supplementary Video S2).

NETs have been shown to foster cancer metastases in cancer models (16). Therefore, we reasoned that the radiation-induced NETs could be also fostering cancer metastasis. To experimentally address this hypothesis, we intravenously injected radiation-induced NETs from human neutrophils that had been previously subjected to mild sonication to avoid clogging in the syringe or in the tail vein, 1 day before the intravenous delivery of 4T1 mCherry-transfected cells. NET preinjection in these mice was conducive to an increase in the number of fluorescent tumor cells detectable in the lungs 10 days later, as shown by the images and their quantitative assessments in Fig. 3G. The metastasis increase effect could have many causative factors. One could be protection from NK cytotoxicity, which reportedly is a relevant factor in these experimental metastatic settings (29). In these mouse experiments, NK depletion with anti-Asialo GM1 resulted in increased lung metastatic burden that was marginally further increased by CD8<sup>+</sup> T-cell codepletion (Fig. 3G). Again, NET preinjection resulted in increased lung metastases, the numbers of which were not further increased by NK or CD8<sup>+</sup> T-cell codepletion (Fig. 3H). To better recapitulate the metastasis process in a model, we performed experiments in a spontaneously metastatic breast cancer model. For this purpose, we intravenously injected mice bearing orthotopically engrafted 4T1mCH fluorescent tumors with NETs isolated from irradiated neutrophils. Other mice received radiation in the contralateral mammary tumor-free gland with respect to the engrafted

orthotopic tumor. Some of these mice were treated with the PAD4 inhibitor GSK484 to inhibit NETosis before radiation of the contralateral mammary glands. Primary tumors were excised, and mice were followed up for 19 days to allow metastasis establishment. Then the lungs of these mice were analyzed for the presence of fluorescent cancer lesions (Supplementary Fig. S2A). In these experiments, injecting radiation-induced NETs promoted the development of more lung metastases. Irradiation of the contralateral mammary gland also gave rise to more numerous lung metastases compared with the control group. This pro-metastatic effect was at least partially inhibited by pharmacologic PAD4 inhibition (Supplementary Fig. S2B and S2C).

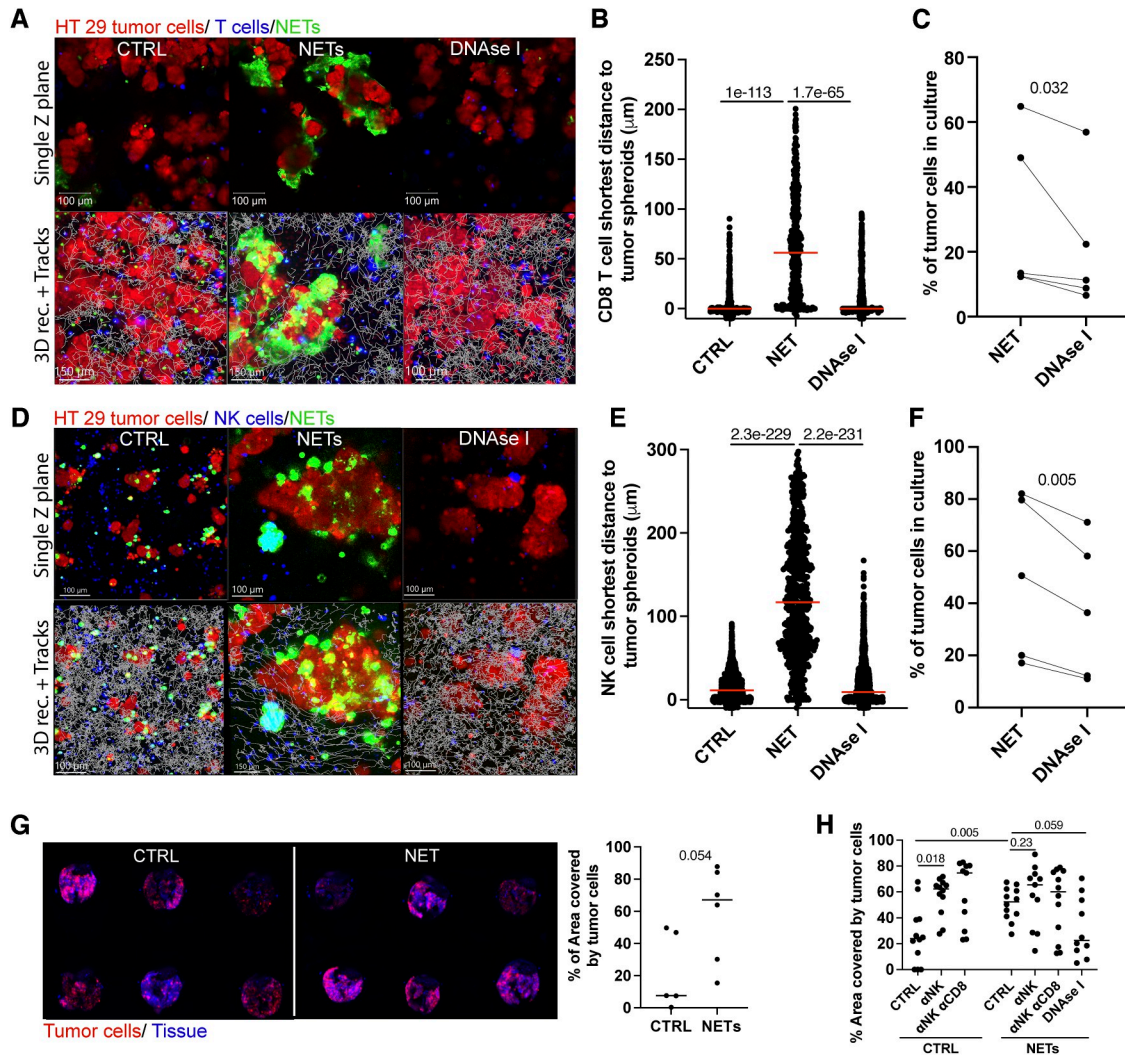
### Increases in circulating NETs in patients with cancer following radiotherapy interventions

Patients with cancer frequently undergo radiotherapy with curative or palliative intent (38). We have set up a method to quantify NETs in solution based on ELISAs, which estimates the concentrations of CitH3 or MPO-conjugated DNA (39). A series of patients undergoing radiotherapy were selected because of having low serum NET concentrations before treatment. Therefore, we excluded patients with high circulating NET levels before treatment (those in the highest quartile). In this way, we could avoid any confounding effects by NETs induced by the malignancy itself (39).

In a first prospective series of 17 patients with a variety of tumors (Supplementary Table S1), blood samples were collected immediately before their first radiotherapy session, 4 to 6 hours after treatment, and/or 24 hours later. In the serum samples, increases in NETs were observed in 8 or 9 of 17 cases using the two ELISA NET-detecting methods (Fig. 4A). These results were validated in a similar second prospective series of 24 patients also selected because of having low circulating NETs before treatment, excluding those cases in the highest quartile (Supplementary Table S1). The ELISA for detecting MPO-DNA complexes showed that 12 of 24 evaluable patients experienced increases, whereas the CitH3 ELISA detected increases in 19 of 24 such cases (Fig. 4B). Analyzing dosimetry curves of some of these treatments made it clear that well-vascularized organs and/or major blood vessels received doses in the range required to elicit NETosis. Figures 4C-H show representative dosimetry cases with an estimate of the volume of blood containing neutrophils that received different intensities of low-dose radiation (1-0.05 Gy) during the course of the first radiotherapy fraction. Representative images show the large blood vessels exposed to indicated dose levels of irradiation.

These results in patients indicated the actual existence of the phenomenon of radiation-induced NETosis at low doses. However, this effect was of a lower magnitude than was expected, according to the *ex vivo* irradiation results. Bearing in mind that *ex vivo* experiments are performed in serum-free media, we reasoned that antioxidants in serum may at least partially quench the induction of NETosis by irradiation (40). Indeed, human serum at a concentration as low as 1% to 3% v/v was able to reduce NET formation (Supplementary Fig. S3A). In the same setting, larger doses of  $\gamma$ -irradiation were capable of overcoming the inhibitory effect of human serum (Supplementary Fig. S3B). Whereas serum albumin was not able to inhibit NETosis (Supplementary Figure S3C), thioredoxin was clearly capable of doing so (Supplementary Fig. S3D), perhaps being a key antioxidant factor (41) in serum and thereby reducing NET formation in the circulation. It must be considered that neutrophils in tumor-bearing hosts are reportedly substantially



**Figure 3.**

Radiation-induced NETs protect tumor cells from cytotoxicity and favor metastasis. **A–E**, HT29 cancer cell spheroids were cultured in the presence of  $\gamma$ -irradiated (2 Gy) neutrophils in the presence/absence of DNase I to allow their coating by NETs for 4 hours. Then, NET-covered or not-covered cancer cell spheroids were cocultured with activated human T cells (**A–C**) or IL2-activated human NK cells (**D** and **E**). **A** and **D**, Representative microphotographs of time-lapse confocal videos (Supplementary Video S2) of such cocultures showing cytotoxic immune cells in blue, tumor cells in red, and NETs (DNA) in green. A representative time point and a single z-slice are shown at the top, and the 3D reconstruction of the whole z-stack that includes the tracks of cytotoxic immune cells is shown below. **B** and **E**, Quantification of the minimum distance of cytotoxic immune cell tracks to tumor cells in the spheroids to account for cell-to-cell interactions with tumor cells. Each dot represents one individual tracked lymphocyte. Mann-Whitney *U*-tests were used for statistical comparisons. **C** and **F**, Percentage of viable tumor cells recovered after 48 hours from such cocultures to account for cytotoxicity. To redirect T-cell-mediated cytotoxicity, 1  $\mu$ g/mL of EpCAM-CD3 $\epsilon$  bispecific Ab (T-cell engager) was added to the cocultures. Pooled data from two to four experiments were analyzed using paired *t* tests. **G**, Balb/c mice were injected twice with mildly sonicated NETs isolated from  $\gamma$ -irradiated human neutrophils, and 24 hours later, 4T1 fluorescent (mCherry<sup>+</sup>) tumor cells were injected in the tail vein of such mice. Representative fluorescence images of the lung of the experimental groups of mice 10 days after tumor cell intravenous injection and quantification of the tumor area on the surface of such lungs. **H**, Experiments were performed as shown in (**G**) but included Ab-based depletion of NK cells (anti-Asialo GM1) and/or CD8<sup>+</sup> T cells (anti-CD8 $\beta$  mAb). Mann-Whitney *U*-tests were used for statistical comparisons.

more susceptible to undergoing NETosis (42) and that cancer-associated neutrophils are usually more immunosuppressive (43).

## Discussion

Our study reveals a phenomenon of the induction of NETosis secondary to low-dose irradiation. The train of underlying mechanisms seems to be the ionization of oxygen molecules that can trigger

the NETosis phenomena in part via activation of NADPH oxidase for secondary waves of  $O_2^{\cdot -}$  production. It has been previously reported that  $O_2^{\cdot -}$  and  $H_2O_2$  functionally trigger the NADPH oxidase enzymatic multiprotein complex (37). We also observe a certain degree of directly or indirectly induced degranulation, which in turn releases IL8 that further stimulates NETosis via CXCR1/2 (3–5) in an autocrine manner. This autocrine IL8-dependent mechanism had not been reported before and

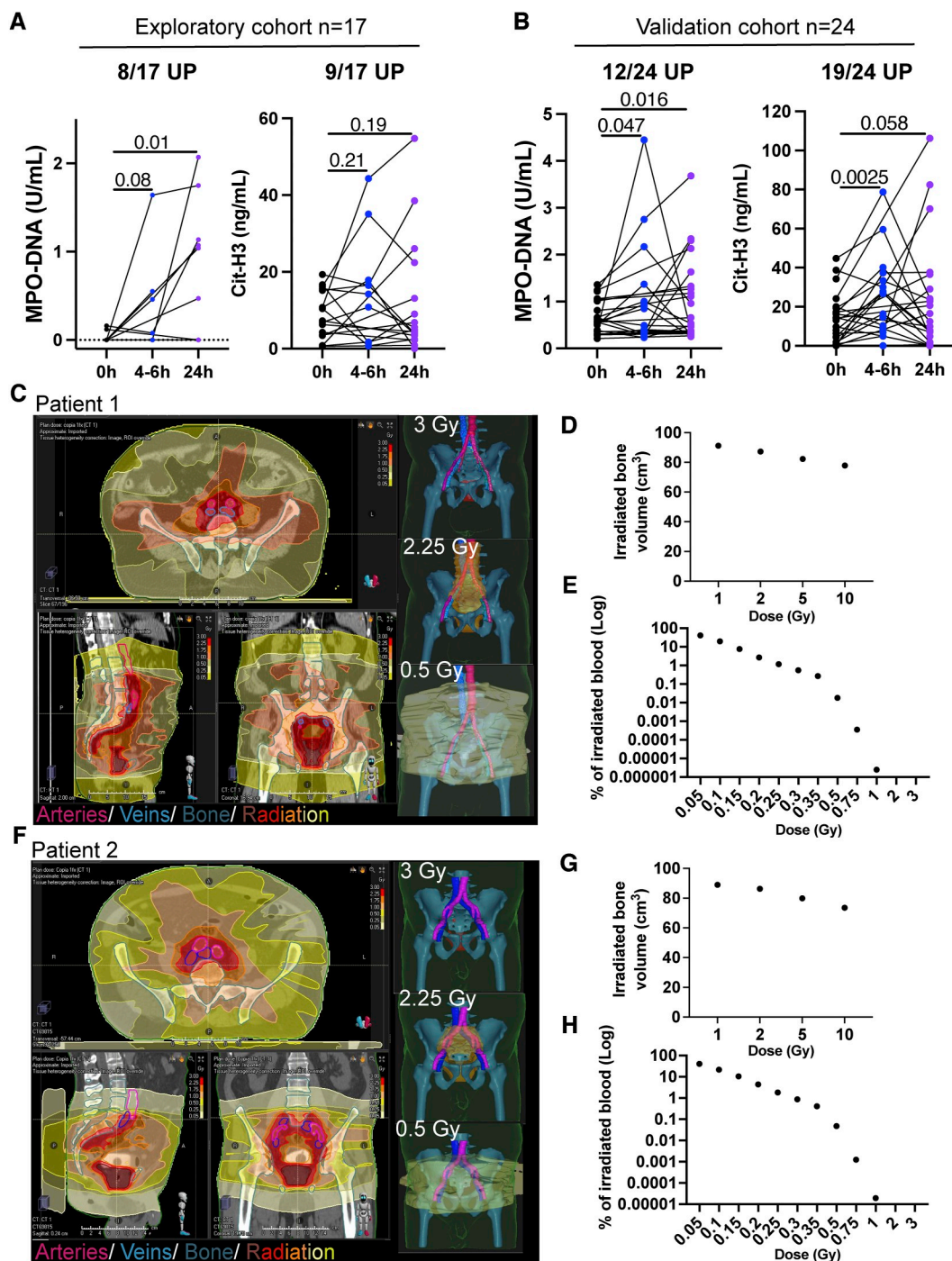


Figure 4.

Patients undergoing radiotherapy experience increases in circulating NETs. Blood of patients with cancer undergoing their first radiotherapy treatments (Supplementary Table S1) was drawn immediately before the radiotherapy session, in some cases 4–6 hours after the radiotherapy treatment and in most cases, 24 hours later. MPO-DNA complexes and CitH3 were measured by ELISAs to quantify circulating NETs in a prospective exploratory cohort (A) and in a second prospective confirmatory cohort (B). Patients with high levels of circulating levels of NETs (the top quartile) prior to radiotherapy were excluded from the analyses to avoid confusion with NETs induced by other factors. The proportion of patients who underwent at least a 30% increase in circulating NETs at any of the time points is indicated above each graph. One-tail paired *t* tests were used to account for statistical significance. C, Images of a representative patient showing the dosimetry curves depicting the amount of radiation received by the tumor lesion and surrounding tissues after one fraction of a radiotherapy course. Isosurfaces in 3D and different 2D projections show the radiated area by different intensities in red to yellow color. Large vessels and bone tissue are overlaid in purple/blue and teal, respectively. D, Bone volume irradiated by the indicated irradiation doses. E, Estimations of the percentage of irradiated blood with the indicated irradiation doses after his/her first single session of radiotherapy are shown. F and H, Representative dosimetry curves (F), percentage of the irradiated bone (G), and estimations of irradiated blood (H) of another patient included in the study.

may have broad implications for inflammatory and malignant conditions.

It should be highlighted that the mechanism of NETosis induction in our experiments is neutrophil-intrinsic. This is in contrast with the reported induction of NETs in the irradiated tumor microenvironment (22). In the case of irradiated tumoral tissue, NETosis was triggered by alarmins released from irradiated tumor cells acting on TLR4 in neutrophils. Whether the neutrophil-intrinsic mechanisms coexist to induce NETosis in the tumor microenvironment would need further investigation.

In patients with cancer who, during tumor-focused radiotherapy, receive low-dose radiation in their circulating blood, the phenomenon of NETosis could be clinically relevant because of potentially pro-metastatic effects, NET-mediated immunosuppression, and procoagulant and prothrombotic activities of NETs (42, 44). NETs will also occur in the tumor itself in which they reportedly are immunosuppressive (45).

We cannot yet ascertain if the detectable circulating increases in patients with cancer and tumor-bearing mice come from the tumor or the circulating neutrophils, especially because of the presence of antioxidative functions in human serum such as those mediated by thioredoxin. Another limitation of this study is that we cannot yet conclude any clinically deleterious effects on the therapeutic outcome of the patients associated with irradiation as mediated by NETosis. To address this important point, large prospective observational studies would be needed to correlate increases in circulating NETs with worse therapeutic results or treatment-related side effects.

Taken together, radiation induces NETosis at very low dose levels. Our mouse experimentation strongly indicates that radiation-induced NETs can act in a protumoral manner. The potential clinical consequences warrant follow-up studies of a series of patients with cancer undergoing radiotherapy in whom circulating NETs could be monitored to determine its putative association with disease outcomes.

## Authors' Disclosures

M. García-Cardosa reports grants from Siemens Healthineers Spain outside the submitted work. J. Burguete reports grants from Siemens Healthineers Spain outside the submitted work. J.L. Perez-Gracia reports grants and personal fees from Astellas; grants from Amgen, Novartis, and Seattle Genetics; grants and nonfinancial support from Bristol Myers Squibb; grants, personal fees, and nonfinancial support from MSD and Roche; and nonfinancial support from Merck outside the submitted work. I. Melero reports grants from AstraZeneca during the conduct of the study as well as grants and personal fees from AstraZeneca, Genmab, Roche, Bristol Myers Squibb, and Boehringer Ingelheim and personal fees from PharmaMar, F-star, Pierre Fabre, HotSpot, Highlight Therapeutics, Bright Peak, Amunix, Curon, Pieris, and Catalym outside the submitted work. No disclosures were reported by the other authors.

## References

- Papayannopoulos V. Neutrophil extracellular traps in immunity and disease. *Nat Rev Immunol* 2018;18:134–47.
- Li P, Li M, Lindberg MR, Kennett MJ, Xiong N, Wang Y. PAD4 is essential for antibacterial innate immunity mediated by neutrophil extracellular traps. *J Exp Med* 2010;207:1853–62.
- Brinkmann V, Reichard U, Goosmann C, Fauler B, Uhlemann Y, Weiss DS, et al. Neutrophil extracellular traps kill bacteria. *Science* 2004;303:1532–5.
- Teixeira A, Garasa S, Gato M, Alfaro C, Migueliz I, Cirella A, et al. CXCR1 and CXCR2 chemokine receptor agonists produced by tumors induce neutrophil extracellular traps that interfere with immune cytotoxicity. *Immunity* 2020;52:856–71.e8.
- Alfaro C, Teixeira A, Onate C, Perez G, Sanmamed MF, Andueza MP, et al. Tumor-produced interleukin-8 attracts human myeloid-derived suppressor cells and elicits extrusion of neutrophil extracellular traps (NETs). *Clin Cancer Res* 2016;22:3924–36.
- Zhan Y, Ling Y, Deng Q, Qiu Y, Shen J, Lai H, et al. HMGB1-mediated neutrophil extracellular trap formation exacerbates intestinal ischemia/reperfusion-induced acute lung injury. *J Immunol* 2022;208:968–78.
- Kirchner T, Moller S, Klinger M, Solbach W, Laskay T, Behnen M. The impact of various reactive oxygen species on the formation of neutrophil extracellular traps. *Mediators Inflamm* 2012;2012:849136.
- Poli V, Zanooni I. Neutrophil intrinsic and extrinsic regulation of NETosis in health and disease. *Trends Microbiol* 2023;31:280–93.
- Wang Y, Wysocka J, Sayegh J, Lee YH, Perlin JR, Leonelli L, et al. Human PAD4 regulates histone arginine methylation levels via demethylation. *Science* 2004;306:279–83.
- Papayannopoulos V, Metzler KD, Hakkim A, Zychlinsky A. Neutrophil elastase and myeloperoxidase regulate the formation of neutrophil extracellular traps. *J Cell Biol* 2010;191:677–91.
- Jorch SK, Kubers P. An emerging role for neutrophil extracellular traps in noninfectious disease. *Nat Med* 2017;23:279–87.

## Authors' Contributions

**A. Teixeira:** Conceptualization, resources, data curation, formal analysis, supervision, funding acquisition, investigation, methodology, writing—original draft, writing—review and editing. **S. Garasa:** Resources, formal analysis, validation, investigation, methodology, writing—review and editing. **M.C. Ochoa:** Investigation, methodology, writing—review and editing. **S. Sanchez-Gregorio:** Investigation, methodology, writing—review and editing. **G. Gomis:** Resources, data curation, investigation, writing—review and editing. **C. Luri-Rey:** Resources, data curation, validation, writing—review and editing. **R. Martinez-Monge:** Supervision, methodology, writing—review and editing. **B. Pinci:** Data curation, investigation, writing—review and editing. **K. Valencia:** Methodology, writing—review and editing. **B. Palencia:** Funding acquisition, project administration, writing—review and editing. **B. Barbés:** Data curation, methodology. **E. Bolanos:** Data curation, investigation, methodology. **A. Azpilikueta:** Formal analysis, validation, investigation, methodology. **M. García-Cardosa:** Data curation, methodology. **J. Burguete:** Data curation, methodology, writing—review and editing. **I. Eiguren-Santamaría:** Resources, investigation, writing—review and editing. **E. Garate-Soraluze:** Methodology, writing—review and editing. **P. Berraondo:** Resources, supervision, writing—review and editing. **J.L. Perez-Gracia:** Resources, methodology. **C.E. de Andrea:** Visualization, methodology, writing—review and editing. **M.E. Rodriguez-Ruiz:** Conceptualization, data curation, formal analysis, supervision, funding acquisition, writing—original draft, writing—review and editing. **I. Melero:** Conceptualization, resources, formal analysis, supervision, funding acquisition, methodology, writing—original draft, writing—review and editing.

## Acknowledgments

We are grateful to Dr. Diego Aligned (flow cytometry unit) for providing support, Sara Fadrique and Haizea Etxebarria for their assistance with dosimetry estimation, Yadira Jimenez for assistance with human sample handling, and Felipe Calvo for scientific discussions. The excellent work of Eneko Elizalde and Elena Ciordia at the animal experimentation service is also acknowledged. This project has been funded by MCIN/AEI/10.13039/501100011033 grant PID2020-113174RA100 (A. Teixeira); MCIN/AEI/10.13039/501100011033 and Fondo Europeo de Desarrollo Regional (FEDER) “Una manera de hacer Europa” grant PID2020-112892RB (I. Melero); FEDER “Una manera de hacer Europa,” the Partners of choice program of AstraZeneca, MCIN/AEI/10.13039/501100011033 and FEDER “Una manera de hacer Europa” grant RYC2019-026406-I (A. Teixeira); Mark Foundation (I. Melero); Fundación La Caixa grant LCF/PR/HR21/00083 (I. Melero); Fundació la Marató de TV3 grant 488/C/2019 (I. Melero); Fundació Fero (I. Melero); Instituto de Salud Carlos III and FEDER grant PI21/01547 (C.E. de Andrea); Fundación CRIS; and Programa Talento Clínico 2020 grant PR\_TCL\_2020 to 2003 (M.E. Rodriguez-Ruiz).

## Note

Supplementary data for this article are available at Clinical Cancer Research Online (<http://clincancerres.aacrjournals.org/>).

Received December 9, 2023; revised March 19, 2024; accepted April 11, 2024; published first April 17, 2024.

12. Hidalgo A, Libby P, Soehnlein O, Aramburu IV, Papayannopoulos V, Silvestre-Roig C. Neutrophil extracellular traps: from physiology to pathology. *Cardiovasc Res* 2022;118:2737–53.
13. Teijeira A, Garasa S, Ochoa MC, Villalba M, Olivera I, Cirella A, et al. IL8, neutrophils, and NETs in a collusion against cancer immunity and immunotherapy. *Clin Cancer Res* 2021;27:2383–93.
14. Nie M, Yang L, Bi X, Wang Y, Sun P, Yang H, et al. Neutrophil extracellular traps induced by IL8 promote diffuse large B-cell lymphoma progression via the TLR9 signaling. *Clin Cancer Res* 2019;25:1867–79.
15. Thalín C, Lundström S, Seignez C, Daleskog M, Lundström A, Henriksson P, et al. Citrullinated histone H3 as a novel prognostic blood marker in patients with advanced cancer. *PLoS One* 2018;13:e0191231.
16. Park J, Wysocki RW, Amoozgar Z, Maiorino L, Fein MR, Jorns J, et al. Cancer cells induce metastasis-supporting neutrophil extracellular DNA traps. *Sci Transl Med* 2016;8:361ra138.
17. Yang L, Liu Q, Zhang X, Liu X, Zhou B, Chen J, et al. DNA of neutrophil extracellular traps promotes cancer metastasis via CDC25. *Nature* 2020;583:133–8.
18. Cools-Lartigue J, Spicer J, McDonald B, Gowing S, Chow S, Giannias B, et al. Neutrophil extracellular traps sequester circulating tumor cells and promote metastasis. *J Clin Invest* 2013;123:3446–58.
19. Albrengues J, Shields MA, Ng D, Park CG, Ambrico A, Poindexter ME, et al. Neutrophil extracellular traps produced during inflammation awaken dormant cancer cells in mice. *Science* 2018;361:ea4227.
20. Mousset A, Lecorgne E, Bourget I, Lopez P, Jenovai K, Cherfils-Vicini J, et al. Neutrophil extracellular traps formed during chemotherapy confer treatment resistance via TGF-beta activation. *Cancer Cell* 2023;41:757–75.e10.
21. Cane S, Barouni RM, Fabbri M, Cuzzo J, Fracasso G, Adamo A, et al. Neutralization of NET-associated human ARG1 enhances cancer immunotherapy. *Sci Transl Med* 2023;15:eabq6221.
22. Shinde-Jadhav S, Mansure JJ, Rayes RF, Marcq G, Ayoub M, Skowronski R, et al. Role of neutrophil extracellular traps in radiation resistance of invasive bladder cancer. *Nat Commun* 2021;12:2776.
23. Najmeh S, Cools-Lartigue J, Giannias B, Spicer J, Ferri LE. Simplified human neutrophil extracellular traps (NETs) isolation and handling. *J Vis Exp* 2015; 98:52687.
24. Knackstedt SL, Georgiadou A, Apel F, Abu-Abed U, Moxon CA, Cunningham AJ, et al. Neutrophil extracellular traps drive inflammatory pathogenesis in malaria. *Sci Immunol* 2019;4:eaaw0336.
25. Sacma M, Matteini F, Mulaw MA, Hageb A, Bogeska R, Sakk V, et al. Fast and high-fidelity *in situ* 3D imaging protocol for stem cells and niche components for mouse organs and tissues. *STAR Protoc* 2022;3:101483.
26. Kessenbrock K, Krumbholz M, Schonermarck U, Back W, Gross WL, Werb Z, et al. Netting neutrophils in autoimmune small-vessel vasculitis. *Nat Med* 2009;15:623–5.
27. Nadler SB, Hidalgo JH, Bloch T. Prediction of blood volume in normal human adults. *Surgery* 1962;51:224–32.
28. Fronck A, Criqui MH, Denenberg J, Langer RD. Common femoral vein dimensions and hemodynamics including Valsalva response as a function of sex, age, and ethnicity in a population study. *J Vasc Surg* 2001;33:1050–6.
29. Spiegel A, Brooks MW, Houshyar S, Reinhardt F, Ardolino M, Fessler E, et al. Neutrophils suppress intraluminal NK cell-mediated tumor cell clearance and enhance extravasation of disseminated carcinoma cells. *Cancer Discov* 2016;6: 630–49.
30. Lewis HD, Liddle J, Coote JE, Atkinson SJ, Barker MD, Bax BD, et al. Inhibition of PAD4 activity is sufficient to disrupt mouse and human NET formation. *Nat Chem Biol* 2015;11:189–91.
31. Bertini R, Allegretti M, Bizzarri C, Moriconi A, Locati M, Zampella G, et al. Noncompetitive allosteric inhibitors of the inflammatory chemokine receptors CXCR1 and CXCR2: prevention of reperfusion injury. *Proc Natl Acad Sci U S A* 2004;101:11791–6.
32. Bilusic M, Heery CR, Collins JM, Donahue RN, Palena C, Madan RA, et al. Phase I trial of HuMax-IL8 (BMS-986253), an anti-IL-8 monoclonal antibody, in patients with metastatic or unresectable solid tumors. *J Immunother Cancer* 2019;7:240.
33. Patel S, Kumar S, Jyoti A, Srinag BS, Keshari RS, Saluja R, et al. Nitric oxide donors release extracellular traps from human neutrophils by augmenting free radical generation. *Nitric Oxide* 2010;22:226–34.
34. Nolan E, Bridgeman VL, Ombrato L, Karoutas A, Rabas N, Sewnath CAN, et al. Radiation exposure elicits a neutrophil-driven response in healthy lung tissue that enhances metastatic colonization. *Nat Cancer* 2022;3:173–87.
35. Ledderose C, Hashiguchi N, Valsami EA, Rusu C, Junger WG. Optimized flow cytometry assays to monitor neutrophil activation in human and mouse whole blood samples. *J Immunol Methods* 2023;512:113403.
36. Paclét MH, Laurans S, Dupre-Crochet S. Regulation of neutrophil NADPH oxidase, NOX2: a crucial effector in neutrophil phenotype and function. *Front Cell Dev Biol* 2022;10:945749.
37. Owusu SB, Hudik E, Ferard C, Dupre-Crochet S, Addison E, Preko K, et al. Radiation-induced reactive oxygen species partially assemble neutrophil NADPH oxidase. *Free Radic Biol Med* 2021;164:76–84.
38. Baskar R, Lee KA, Yeo R, Yeoh KW. Cancer and radiation therapy: current advances and future directions. *Int J Med Sci* 2012;9:193–9.
39. de Andrea CE, Ochoa MC, Villalba-Esparza M, Teijeira A, Schalper KA, Abengozar-Muela M, et al. Heterogenous presence of neutrophil extracellular traps in human solid tumours is partially dependent on IL-8. *J Pathol* 2021; 255:190–201.
40. Inoue M, Nakashima R, Enomoto M, Koike Y, Zhao X, Yip K, et al. Plasma redox imbalance caused by albumin oxidation promotes lung-predominant NETosis and pulmonary cancer metastasis. *Nat Commun* 2018;9:5116.
41. Lu J, Holmgren A. The thioredoxin antioxidant system. *Free Radic Biol Med* 2014;66:75–87.
42. Demers M, Krause DS, Schatzberg D, Martinod K, Voorhees JR, Fuchs TA, et al. Cancers predispose neutrophils to release extracellular DNA traps that contribute to cancer-associated thrombosis. *Proc Natl Acad Sci U S A* 2012; 109:13076–81.
43. Coffelt SB, Wellenstein MD, de Visser KE. Neutrophils in cancer: neutral no more. *Nat Rev Cancer* 2016;16:431–46.
44. Rosell A, Martinod K, Mackman N, Thalín C. Neutrophil extracellular traps and cancer-associated thrombosis. *Thromb Res* 2022;213:S35–41.
45. Zhang Y, Chandra V, Riquelme Sanchez E, Dutta P, Quesada PR, Rakoski A, et al. Interleukin-17-induced neutrophil extracellular traps mediate resistance to checkpoint blockade in pancreatic cancer. *J Exp Med* 2020;217: e20190354.